LUND UNIVERSITY

Methods to Generate Size- and Composition Controlled Aerosol Nanoparticles

Karlsson, Martin

2004

[Link to publication](#)

Total number of authors:
1

Methods to Generate
Size- and Composition Controlled
Aerosol Nanoparticles

Martin Karlsson

Division of Solid State Physics
Lund 2004

Doctoral Thesis

LUND INSTITUTE OF TECHNOLOGY
Lund University

Utan tvivel är man inte klok.

—Tage Danielsson

Abstract

This thesis describes experiments performed using different methods to produce aerosol nanoparticles with control over size and composition. The process included differential mobility analyzers (DMAs) as size-selecting instruments and tube furnaces for particle synthesis.

A method to estimate the degradation of the DMA performance from the ideal case for individual DMAs was proposed and tested experimentally. Using this method, the size dependence of the DMA performance was predicted from measurements at a single particle size.

Size- and composition controlled binary alloy aerosol nanoparticles were generated. Core particles were formed by the evaporation/condensation method, and alloy particles were created by the subsequent condensation of another material. The Au-Ga system was used as a test system.

Generation processes were investigated by studying deposition patterns inside a horizontal evaporation/condensation nanoparticle generator. Comparison to estimates calculated from a one-dimensional monodisperse aerosol formation model indicates the presence of non-uniform flow inside the generator.

Aerosol nanoparticles were created from the vapor emanating from the thermal decomposition of iron pentacarbonyl. The size, morphology, composition and structure of the generated iron-containing particles were investigated.

The sintering behavior of agglomerated aerosol nanoparticles was investigated. When comparing the relative compaction temperature for different nanoparticles produced in different laboratories deviations in the sintering behavior were found. These could be associated to the different particle compositions.

Individual nanoparticles were generated from monodisperse colloidal suspensions by the use of an electrospray method. Deposition of single particles could be achieved and controlled by deposition time and dilution ratio. The method was found to be independent of particle material.

Preface

This thesis is a summary of the work I have completed as a Ph.D. student at the Department of Physics in Lund during the years 1999 and 2004. The thesis consists of introductory chapters presenting general aspects of the topics discussed in detail in the six amended research papers.

Contrary to the usual case for a Ph.D. student, I have had the pleasure to experience two Divisions. I have however been loyal to aerosol science all the time. I started out at the Division of Nuclear Physics, where I mostly performed experiments on characterizing an instrument called a Differential Mobility Analyzer, or DMA[1] for short. The aim was to develop methods which could be used for measuring atmospheric aerosols. The work resulted in the first two papers in this thesis. In early 2001, I turned the focus towards aerosol nanoparticles and started at the Division of Solid State Physics. Using an experimental set-up including a similar instrumentation, I began producing nanometer-sized particles of different materials. The aim was to develop new methods for generating particles that could find applications in the field of nanotechnology. The results of the work are presented in the four last papers included in this thesis. To summarize, it has been both enjoyable and educating to work with similar instruments and similar research problems from two different points of view!

There are a number of people who have helped in one way or another along the way, which of course are gratefully acknowledged.

First, I would like to express my warmest gratitude to my thesis advisor Prof. Knut Deppert, whom I regard more as a fellow Ph.D. student than a supervisor. Working with (i.e., not for) you has always been a great joy, and your positive spirit about science and all else that matters have encouraged me significantly. Thanks for a great cooperation!

Also, I would like to thank Prof. Lars Samuelson who accepted me as a Ph.D.

---

[1]Get used to this TLA (three letter acronym) if you intend to read the entire thesis!

List of papers

This thesis is based on the following publications, referenced to in the introductory chapters as Papers I to VI.

I

Methodology to estimate the transfer function of individual differential mobility analyzers
Bengt G. Martinsson, Martin N.A. Karlsson, and Göran Frank
Aerosol Science and Technology **35**, 815 - 823 (2001)

In this paper, a method to estimate the degradation of the differential mobility analyzer (DMA) transfer function from the ideal case for individual DMAs of unknown characteristics is described. The proposed method was tested experimentally and managed to explicitly estimate the DMA transfer functions via two independent parameters. My contribution was to plan and perform most of the experiments, and assist in writing the paper.

II

Methods to measure and predict the transfer function size dependence of individual DMAs
Martin N.A. Karlsson and Bengt G. Martinsson
Journal of Aerosol Science **34**, 603 - 625 (2003)

In this paper, the size dependence of the DMA transfer function was investigated, using the method described in Paper I. Methods to predict the size dependence of the two involved parameters were proposed and verified experimentally. The

results indicated that the size dependence of the transfer function in total can be estimated from measurements at a single particle size. I contributed in the planning of and performed the experiments, and wrote the paper.

III

Size- and composition controlled Au-Ga alloy aerosol nanoparticles
Martin N.A. Karlsson, Knut Deppert, Lisa S. Karlsson, Martin H. Magnusson and Jan-Olle Malm
Manuscript submitted 2003-12-09 to *Aerosol Science and Technology*

In this paper, a method for size- and composition controlled production of binary alloy aerosol nanoparticles was developed. The method includes the formation and classification of one material and the subsequent condensational addition of another. The Au-Ga system was used as a test system, and core-shell particles could be formed under certain conditions. My contribution was to plan and perform the experiments producing the binary alloy nanoparticles, and to write the paper.

IV

Experimental evidence for non-uniform flow in a horizontal evaporation/ condensation aerosol generator
Ted A. Damour, Sheryl H. Ehrman, Martin N.A. Karlsson, Lisa S. Karlsson, and Knut Deppert
Manuscript intended for *Aerosol Science and Technology*

In this paper, deposition patterns inside a horizontal evaporation/condensation nanoparticle generator were studied for four different metals: indium, gallium, silver, and lead. These patterns were compared to estimates calculated from a one-dimensional monodisperse aerosol formation model. Both the observed depositions and the results of the comparison indicate the presence of non-uniform flow inside the generator, which affect the particle formation. My contribution was to perform the scanning electron microscope analysis, to assist in some experiments and in preparing the manuscript.

V

Size-controlled nanoparticles by thermal cracking of iron pentacarbonyl
Martin N.A. Karlsson, Knut Deppert, Brent A. Wacaser, Lisa S. Karlsson, and Jan-Olle Malm
Manuscript submitted 2004-02-27 to *Applied Physics A*

In this paper, a method to produce nanoparticles from the vapor emanating from the thermal decomposition of iron pentacarbonyl, and subsequent compaction of the size-selected particles was developed. The size, morphology, composition and structure of the generated particles, and the temperature dependence of these properties were investigated. My contribution was to plan and perform the experiments producing the nanoparticles, and to write the paper.

VI

Material related sintering behavior of nanoparticles: an evaluation of experimental data
Martin N.A. Karlsson, Knut Deppert, Lisa S. Karlsson, Martin H. Magnusson, Jan-Olle Malm, and N.S. Srinivasan
Manuscript submitted 2004-04-16 *Journal of Nanoparticle Research*

In this paper, the sintering behavior of agglomerated aerosol nanoparticles of different material produced by different laboratories was investigated. When comparing the data, the relative compaction temperature of three metals and two semiconductors was found to differ significantly from the temperature of titania. My contribution was to assist in the data collection and writing the final paper.

Martin Karlsson

Contents

Chapter 1

Introduction

Producing nanometer-sized particles with sufficient control of properties, such as size and composition, and in large enough quantities is of great interest for many applications. This thesis explored different generation methods based on aerosol technology. The instrumentation for measuring different particle properties is described. Size determination is given the most attention since the size is often the most important characteristic for nanoparticles.

The main instrument for measuring aerosol particle size on-line is called the differential mobility analyzer (DMA). A considerable part of this thesis deals with the performance of this instrument and especially its so-called transfer function. Since a DMA is a classification device, it is used extensively in experimental set-ups used for particle production. In this thesis, a generator set-up including DMAs were used for the production of aerosol nanoparticles.

1.1 Definition of aerosol

An aerosol is defined as solid or liquid particles suspended in a gas [1]. The gas is normally but not necessarily air. The term aerosol includes both the particles and the surrounding gas, thus making it a system of two or even three aggregation phases. The term particle refers both to the solid particles and the liquid particles. The latter are often referred to as droplets. The size of the particles ranges from 1 nm to 100 μm, covering five orders of magnitude. The minimum size is limited by the fact that a particle must be composed of a stable assembly of atoms or molecules. The maximum size is limited by the settling velocity of the particle due to gravity. Larger particles will simply fall downwards too rapidly to be

Table 1.1: Types of particulate suspensions (after ref. [1]).

Suspending medium	Type of suspended particles		
	Gas	Liquid	Solid
Gas	—	Fog, mist, spray	Fume, smoke, dust
Liquid	Foam	Emulsion	Colloid, slurry
Solid	Sponge	Gel	Alloy

considered airborne. The definition of an aerosol implies that nearly all gases can be considered to be aerosols, since there are practically always particles present. However, in the normal case only the suspended particles are of interest and the surrounding gas is neglected. This has unfortunately led to the reinterpretation of the term aerosol to only include just the particles. In a popular context, the term aerosol often refers to a pressurized can product as a whole, but it is actually the material coming out of the can that is the aerosol.

In fact, an aerosol is just one example of a particulate suspension. The term was coined as an analog to the term hydrosol, which refers to a stable liquid suspension of particles. All two-component system made up of particles of one component in a stable suspending medium of another component have unique properties that depend on the size of the particles and the relative concentrations. Each of these systems have names, which are listed in Table 1.1. The aerosols listed in the table are found in the upper row. The difference between the different terms are the size of the particles and their method of generation. For instance, consider the listed aerosols of solid particles. A fume emanates from the condensation of a vapor and consists therefore of particles less than 50 nm. Smoke arises as a result of incomplete combustion, and the particles are usually less than 1 μm. Lastly, dust particles are formed by mechanical disintegration such as crushing and grinding, and consists mainly of particles larger than 100 μm.

Scientific work with aerosols is often synonymous with pollution control. This deals with reducing particle concentrations and controlling particle emissions in order to prevent humans the harmful effects of aerosols. There are of course other specific applications which are benefited by the properties of aerosol particles. Clean room technology is an example where the control and reduction of aerosol particles is used to protect the products manufactured in such rooms,

rather than the humans working there. Another example is the pressurized spray technique, which among other things is used for applying pesticides, distributing paint droplets or even spraying perfume. Other important and widespread uses of aerosol particles have medical applications [2]. Apart from the control of unintentional exposure of aerosols to humans, e.g., during surgery, aerosol particles can be used both for therapeutic and diagnostic purposes. Therapeutic aerosols are often intended for inhalation, aiming to deliver a substance to the respiratory tract. For instance, aerosol particles can be used to alter the properties of secretion or treat infections. The aerosols can be generated from pulverized drugs, as in the case of asthma medication intended for deposition in the lungs. They can also be sprayed from a solution, as with medication intended for deposition in the nasal region. Aerosols can also be used for diagnostic purposes such as assessment of the ventilation of the lungs, e.g., using nuclear medicine techniques. Many of these applications are often critically dependent on the properties of the aerosol being used. This makes it important to perform precise characterizations of aerosols, as will be discussed in depth in Chapter 2.

1.2 Aerosol nanoparticles

The field of aerosol technology has drawn increasing attention from nanotechnologists, in particular the possibility for accurate size measurements and controlled generation. Nanotechnology is a discipline dealing with fabrication, physics and manipulation of nanostructures, which includes nanoparticles. Particles smaller than 100 nm are normally considered to be nanoparticles. Just by their small size they may have electrical, optical, magnetic, and/or chemical properties which differ from that of the corresponding bulk material. As a result, the novel properties of nanoparticles makes them interesting for a variety of new uses [3]. For example, nanoparticles can be used as quantum dots in studies making use of quantum confinement effects [4, 5], in luminescent materials for integration in optoelectronic devices [6], as part of gas sensors for converting microscopic chemical interactions into measurable electrical signals [7], and as UV blocking pigments in solar protection creams or films preventing color degradation of plastics [8].

The different particle properties are highly dependent on the size of the particle. Nanoparticles are typically larger than molecules but smaller than bulk solid-state structures. This means that the preparation process must be highly accurate. Important preparation qualities include good control of particle size and shape, and monodispersivity within a few percent. Processes involving aerosols can re-
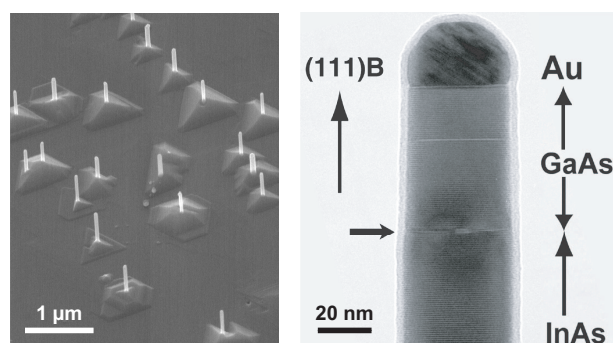
Figure 1.1: (Left) An SEM overview image of GaAs whiskers. (Right) A TEM image of a 40 nm whisker with an InAs/GaAs interface, indicated by an arrow. From Ref. [9]

spond well to these demands since the processes take place in the gas phase. This makes for instance particle size control easy. Gas phase production has several advantages including the potential to create particles that are metal, binary alloy or even more complex chemical structures. Aerosol nanoparticles are essentially formed by condensing individual atoms into small solid building blocks. Control of the gas flows leads to high purity production of nanoparticles and offers a possibility to have continuous production. Major disadvantages are limited yield of the generation, problems associated with storage and costly experimental equipment. Colloidal nanoparticles is an alternative particle technology which can overcome these disadvantages. Producing particles in a solution can be done in large amounts at a low cost, and the particles can easily be stored and transported. However, size selection is more difficult to achieve for colloidal suspensions, and the particle purity is often lower than compared to aerosol particles.

As a specific application, aerosol nanoparticles can act as seeds for epitaxial growth of semiconductor nanowhiskers, one-dimensional nanostructures [10]. To grow whiskers, size-selected particles of for instance Au are first deposited onto a substrate. The substrate is then transferred to a growth chamber, e.g., a chemical beam epitaxy chamber, and heated while exposed to gaseous growth species. These are dissolved in the catalysts and whiskers start to grow in the catalyst-semiconductor interface due to supersaturation in the metal droplet. Heterostructures can be fabricated by changing the gaseous species. Fig. 1.1 shows an scanning electron microscope (SEM) image of GaAs whiskers approximately 500 nm in length, and a transmission electron microscope (TEM) image of a heterostructure whisker. The gold aerosol nanoparticle is clearly seen at the top.

Chapter 2

Aerosol nanoparticle measurement

The most important parameter for nanoparticle characterization is size. All other aerosol properties depend upon size, some very strongly. For instance, all forces acting on particles depend upon size. In some cases the governing laws themselves may change with particle size. Aerosol nanoparticles, having sizes which are close to the surrounding gas molecules, react differently with the suspending gas than larger particles, for which the gas can be treated as a continuum. Therefore, it is always important to measure size with great accuracy. Most of the size measurement techniques infer particle size indirectly from an observation of some particle behavior. In order to minimize ambiguity, size measurements are often reported in terms of equivalent diameters.

The main instrument for making size measurements of aerosol particles, especially in the nanometer size range, is the differential mobility analyzer. This instrument is described in detail in section 2.2. Other aerosol instruments that measure size distributions and number concentrations of particles are described in section 2.3.

2.1 Equivalent diameters

In the development of the theory of aerosol properties it is often assumed that the particles are all spherical, since this makes the theories more simple. However, in reality aerosol particles are often highly non-spherical, which makes it rather

difficult to define a diameter. In order to extend the aerosol theories to encompass non-spherical particles, the concept of equivalent diameter has been introduced. An equivalent diameter is the diameter of a sphere that has the same value of a particular physical property. For instance, the equivalent volume diameter is the diameter of a sphere having the same volume as that of the irregular particle. The equivalent volume diameter can be thought of as the diameter of the sphere that would result if the irregular particle would melt to form a droplet. Another, and more important equivalent diameter, is the aerodynamic diameter. The aerodynamic diameter standardizes both shape and density. It is defined as the diameter of a spherical particle with a density of 1000 kg/m^3 that has the same settling velocity as the irregular particle. The settling velocity is the terminal velocity of a particle settling in still gas. It is a condition of constant velocity wherein the drag force of the gas on the particle is exactly balanced by the force of gravity. In this context, the particle property mobility can be defined as the ratio between the terminal velocity and the steady force producing that velocity. If the force is gravitational, the mobility is called the mechanical mobility, B. Further, for charged particles moving in an electric field, the electrical mobility, Z, can be defined as the ratio between the terminal velocity caused by the electric field and the electric field. The electrical mobility diameter is now defined as the diameter of the spherical particle having the same electrical mobility as the particle of interest. The electrical mobility diameter for a spherical, singly charged particle is the same as the geometric diameter. The concept of electrical mobility will be further discussed in section 2.2.

Equivalent diameters can also be defined for the geometry of the particle silhouette, such as Martin's or Feret's diameter. These are useful for microscopic measurements of particle sizes. The most commonly used equivalent diameter is however the projected area diameter, which is defined as the diameter of the circle having the same projected area as the particle of interest.

2.2   The differential mobility analyzer

A differential mobility analyzer (DMA) is an instrument which classifies particles according to their electrical mobility. It was introduced by Knutson and Whitby in 1975 [11] and has ever since become a standard tool in aerosol science, appearing in a variety of applications. The great advantage with a DMA is its possibility to act as a gate by extracting aerosol particles with a narrow mobility range from a distribution of particles with different mobilities. This range can thereafter be

treated in different ways according to the purpose of the application. There are two main applications for a DMA. It can be used both as a part of a particle size measuring system and as a part of a particle generation system.

One common system for measuring particle size distributions is the differential mobility particle spectrometer (DMPS) [12]. The particles in the selected range are counted either by a CPC or by an electrometer. A size distribution is then obtained by varying the voltage of the DMA. The DMPS provides precise measurements of particle size distributions with high resolution in the sub-micrometer size range. It can, for example, be used to measure atmospheric particle size distributions [13].

An example of a more complex measurement system including two DMAs is the tandem DMA (TDMA). A TDMA employs two DMAs in series. The particles with a mobility range selected by the first DMA are exposed to a region of controlled conditions. Subsequently, the second DMA is used to measure the change in mobility, hence making it possible to study processes that change particle size. For instance, if the particles pass a region of controlled relative humidity between the DMAs, the hygroscopic particle growth can be studied [14]. In analogy to spectroscopy, the first DMA held at a fixed voltage could be compared to a monochromator. The second DMA which scans over the distribution produced by the first is analogous to a spectrometer. There are also more sophisticated measurement system, which includes several DMAs, such as a droplet aerosol analyzer (DAA) [15]. A DAA is used to perform correlated measurements of cloud droplet size and droplet residual particle size [16].

The other main use of a DMA is as part of a monodisperse aerosol generator to produce particles with a narrow mobility range. An aerosol with a certain particle size distribution is first created. This can be done by using a constant output atomizer [17] or by rapid cooling of a supersaturated vapor, called the evaporation/condensation method [18]. The aerosol is then passed through a DMA operated at a fixed voltage, generating the monodisperse particles. This use of a DMA for particle generation was the most important method used in the experiments in this thesis. This method will therefore be described further in Chapter 3.

2.2.1   The physical principle

The DMA classifies individual aerosol particles according to their electrical mobility Z_p. The electrical mobility can be defined as the ability for a charged particle

to move in an electrical field [1]. Z_p depends on the charge ne, where n is an integer and e is the elementary charge of an electron, and the diameter d_p of the particle. The electrical mobility can be expressed as the ratio between the terminal electrostatic velocity V_{TE} and the electrical field strength E

$$Z = \frac{V_{TE}}{E} = \frac{neC_c}{3\pi\eta d_p} \tag{2.1}$$

Here, η is the viscosity of the surrounding gas and C_c is the so called Cunningham factor. The viscosity depends on temperature according to

$$\eta = \eta_0 \left(\frac{T}{T_0}\right)^{1/2} \tag{2.2}$$

where $\eta_0 = 1.83 \times 10^{-5}$ kg/m·s and T_0 = 293 K. The Cunningham factor C_c is also called the slip correction. It accounts for the fact that the surrounding gas cannot be regarded as a continuum for small particles, i.e., when the particles are of the same order of magnitude in size as the mean free path. It is given by

$$C_c = 1 + \frac{\lambda}{d_p}\left[2.34 + 1.05\exp\left(-0.39\frac{d_p}{\lambda}\right)\right] \tag{2.3}$$

where λ is the mean free path. This in turn is a function of the temperature T and pressure p of the gas, and is given by

$$\lambda = \lambda_0 \left(\frac{T}{T_0}\right)\left(\frac{p_0}{p}\right) \tag{2.4}$$

where $\lambda_0 = 6.53 \times 10^{-8}$ m and p_0 = 1013 hPa. For a particle with a diameter of 1 μm, the Cunningham factor becomes 1.15 (at standard temperature and pressure, i.e., T_0 and p_0), and the factor increases with decreasing particle size. In total, the electrical mobility of a particle depends primarily on its diameter and charge, and implicitly on the temperature and the pressure of the surrounding gas, through the viscosity and the Cunningham factor. Thus, by measuring the electrical mobility of particles of a known charge distribution, and knowing the gas temperature and pressure, the diameter of the particles can be derived.

In a DMA, charged aerosol particles pass through a parallel plate capacitor in which particle penetration is controlled by an electric field. The two most common DMA types have radial or cylindrical design, respectively. In a radial DMA, an electrical field is generated between two parallel circular discs [19, 20].
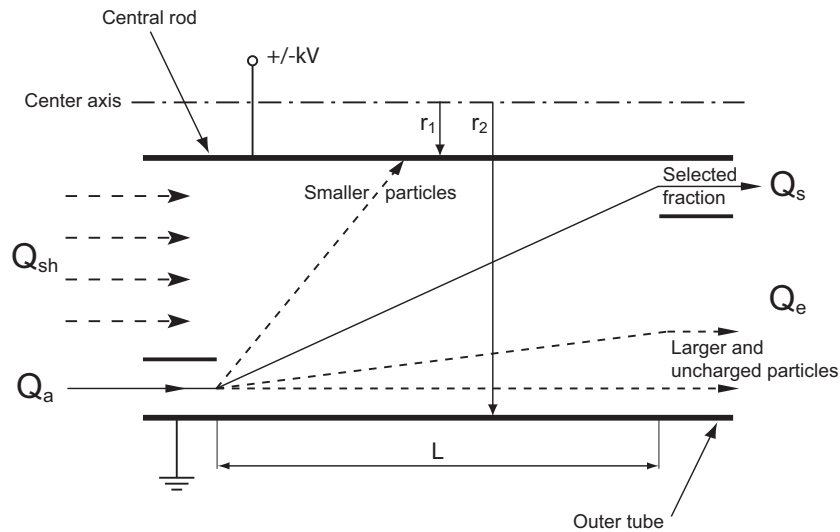
Figure 2.1: Schematic cross section diagram of a cylindrical DMA.

The aerosol enters the space between the discs at the periphery and travels towards the center. This DMA design has not been investigated in the work presented in this thesis.

In a cylindrical DMA, a radial electric field is generated between a tube and a central electrode rod. The tube is grounded and the voltage of the central rod can be varied between approximately 10 V and 10 kV. Fig. 2.1 shows a schematic cross-sectional view of a cylindrical DMA (see also Fig. A.1). The polydisperse aerosol flow (Q_a) is introduced axially through a fine slit in the outer annulus. In contrast, the laminar and particle-free sheath gas flow (Q_{sh}) enters the DMA in the center. Before entering, the sheath gas flow passes a woven wire mesh which induces a pressure drop. This drop distributes the flow evenly over the DMA cross section. As the two flows travel axially between the coaxial tube and the central rod, the charged aerosol particles having the appropriate polarity are deflected towards the central rod. Only those particles with a narrow range of electrical mobility will be carried out by the minor, nearly monodisperse sampling flow (Q_s) through the narrow exit slit. Smaller and multiply charged particles have greater mobility and will therefore migrate to the central rod before reaching the exit slit. Larger, uncharged, and oppositely charged particles on the other hand have lower mobility, and will therefore follow the excess flow (Q_e) out of the

Table 2.1: Bipolar equilibrium charge distribution as calculated with the model presented by Wiedensohler [21]. The table gives the percentage of particles carrying the indicated number of charges.

d_p (nm)	−3	−2	−1	0	+1	+2	+3
10	0	0	5.1	91.2	4.1	0	0
20	0	0	11.0	79.3	8.5	0	0
50	0	1.1	22.3	58.1	17.0	0.7	0
100	0.4	5.6	27.9	42.6	21.4	3.2	0.2

instrument. However, not all particles in the selected mobility range will leave the DMA with the sampling flow. This will be adressed in section 2.2.3.

2.2.2 Charging

Most of the aerosol particles in ambient air are naturally charged. This can be a result of either their generation process or the adhesion of ions. However, natural charging of particles are seldom in the well-ordered manner required for making mobility measurements. Instead, bipolar chargers are frequently used to charge aerosol particles. Bipolar chargers give the aerosol a known charge distribution, a process sometimes called neutralization. The charger used in the work presented here makes use of the ionizing radiation from a radioactive source, e.g., β-emitting ^{63}Ni, to ionize the gas in a confined region. When the aerosol passes this ionized volume, ions of both polarities will collide randomly with the aerosol particles. As they attract oppositely charged ions, this charges the particles that are neutral and neutralize the particles that are charged. After a sufficient amount of time, typically about one second, the aerosol reaches an equilibrium charge state. The equilibrium can be described as the statistical probability that some aerosol particles will have no charge and others will have one or more charges. Wiedensohler [21] derived by polynomial fitting an approximate and asymmetric distribution, which is shown in Table 2.1. Since the equilibrium charge distribution is well defined, inversion techniques can be used to convert measurements of electrical mobility into particle size.

2.2.3 The transfer function

The DMA transfer function is defined as the particle penetration as a function of the electrical mobility for a given voltage and flow setting. In other words, it is the probability that a charged aerosol particle entering the instrument via the aerosol inlet will leave it via the sampling flow. The transfer function for cylindrical DMAs can be derived by considering the two perpendicular forces experienced by particles entering the DMA. These are the axial force caused by the gas flow and the radial force caused by the electric field. This derivation is performed in the Appendix.

Particles selected by a DMA have a narrow electrical mobility distribution. The mean electrical mobility, Z_p^*, of the particles leaving the DMA with the sampling flow can be derived by realizing that the axial and radial traveling times for those particles are equal. For a DMA operated with symmetrical flows, which is the normal case, Z_p^* becomes

$$Z_p^* = \frac{Q_{sh}ln(r_2/r_1)}{2\pi UL}. \tag{2.5}$$

where r_1 and r_2 are the radii of the electrode rod and the outer cylinder, respectively, U the applied voltage and L the length of the DMA classifier column (cf. Fig. A.1). The relative full width of the mobility range is the full width, ΔZ_p, divided by Z_p^*. It becomes

$$\frac{\Delta Z_p}{Z_p^*} = 2\frac{Q_a}{Q_{sh}} \tag{2.6}$$

and the transfer function becomes symmetrical and triangular, as depicted in Fig. 2.2. In the ideal case, the shape of the transfer function is determined only by the applied flow rates. The ideal full width of half maximum, or resolution, thus becomes Q_a/Q_{sh}. The transfer function shape can however be degraded and become non-ideal due to several factors. Factors contributing to degradation include flow rate maladjustments, imperfections in the design of the DMA and presence of an unwanted electric field at the DMA outlet. The first two of these factors can cause a formation of a non-laminar flow field in the DMA, especially in the region where the aerosol flow and the sheath gas flow meet. Particle losses are most likely to occur at the inlet and outlet of the DMA.

In addition to DMA imperfections, the shape of the transfer function is affected by diffusion. Diffusion is the random collisions between particles and the molecules in the gas. This randomness causes particles inside a DMA to deviate
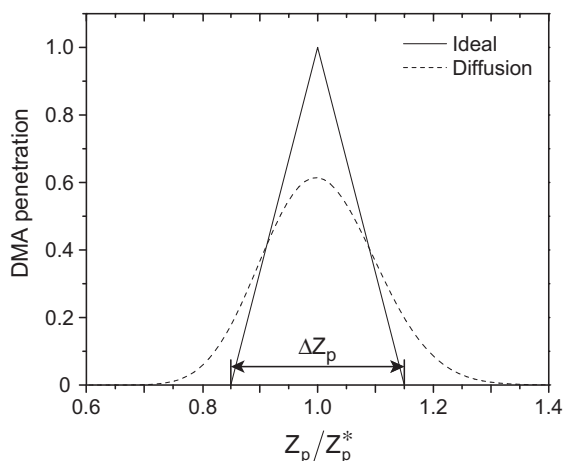
Figure 2.2: The ideal (solid line) and diffusionally broadened (dashed line) differential mobility analyzer transfer function as a function of the ratio of the mobility Z_p to the mean mobility Z_p^*. Both functions are calculated with $Q_a/Q_{sh} = 0.15$. The diffusionally broadened transfer function is calculated by using a derived analytical function [22] together with DMA parameters $Q_{sh} = 6$ l/min, $Q_a = 0.9$ l/min, $L = 0.28$ m, and $d_p = 13$ nm.

from the theoretical trajectories determined by the axial gas flow and the radial electric field. Effectively, this broadens the transfer function as compared to the ideal case. This diffusional broadening makes it difficult to obtain narrow size distributions. Stolzenburg [22] derived analytical expressions describing the influence of diffusion on the DMA transfer function. On the basis of DMA properties such as aerosol and sheath gas flow rates, applied voltage, length, radii, and the diffusion coefficient, it is possible to estimate the diffusion broadened transfer function. In Fig. 2.2, the ideal and the diffusion corrected size distribution is plotted for an aerosol-to-sheath gas flow-rate ratio of 0.15. The diffusional transfer function is clearly broadened compared to the ideal case. Further, it should be noted that the diffusional transfer function is not symmetric. This is because diffusion is dependent on particle size, in that smaller particles are more effected by diffusion than larger.

The transfer function shape is also affected by losses due to DMA imperfections, as previous mentioned. These losses cause measurements of particle size distributions to become non-quantitative when not accounted for. For example, this can be a problem when performing measurements with a DMPS since there

will be fewer counts in each size channel.

It is not realistic to construct perfect DMAs with ideal transfer functions. Therefore one is forced to measure the transfer functions and correct the experimental data. Size dependencies of the diffusion and the losses due to DMA imperfections are instrument-specific and constant for all measurements. These constants can, if they are known, then be used to correct the experimental data.

In Paper I, a method to estimate the non-ideal features of the DMA transfer function is presented and experimentally tested. In Paper II, investigations of the size dependence of the transfer function using this method are reported. The work presented in these papers could thus be useful for DMA users and perhaps also for DMA constructors.

2.3 Methods for sizing and counting

Size and number concentrations are important properties for particle characterization. There are therefore a variety of instruments based on different principles measuring these properties. In this section, some of these instruments will be described. Not all of them are relevant to the field of nanoparticles, but are nevertheless described since they are used frequently in aerosol science.

2.3.1 Impactor

An impactor is an instrument which separates particles according to their inertia by selective collection, or impaction. An illustrative example of a collector is the windshield of a car. Large insects impact with the windshield, as they fail to follow the air streamlines of the moving car. On the other hand, snowflakes easily escape impaction due to their smaller size, unless the speed of the car is high.

In an impactor, the aerosol of interest is passed through a nozzle, forming a jet of particles, which is directed against a flat impaction plate perpendicular to the flow. Particles whose inertia exceeds a certain value will collide with the plate, or impact. Only those particles able to follow the gas streamlines will remain airborne and leave the instrument. Thus, the particles will be divided into two size ranges, with the limit at a certain cutoff aerodynamic diameter. By changing the distances involved, and especially the diameter of the nozzle, this limit can be altered. The two determining factors whether particles will impact or not is the gas flow rate and the particle size.

In its simplest form, the impactor only consists of a single step, but there are

also so called cascade impactors, with several stages of impactors in series. The cutoff size is reduced at each stage by decreasing the nozzle size. The impaction plates can for instance be analyzed gravimetrically in order to deduce a particle size distribution. A so called virtual impactor has been developed in order to overcome problems such as resuspension of impacted particles and plate overloading. The impaction plate is in this case replaced by a minor collection flow, hence the term virtual. The collection flow separates the impacted particles according to a certain aerodynamic cutoff diameter through a nozzle pointing in the opposite direction as the contraction nozzle.

Impactors have the advantage of being simple, both in construction and operation, and have therefore become a standard tool in aerosol science. However, it is difficult to sample small particles, since the smaller the particles, the higher the gas flow rate, which in turn leads to higher probability of particle bounce. Conventional impactors are limited to measure particles with sizes larger than approximately 0.5 μm, which makes them unsuited for nanoparticle measurements. However, a nanoparticle virtual impactor able to collect particles with sizes ranging from 15 to 60 nm with a collection efficiency of 50% was presented in a recent study [23].

2.3.2 Time-of-flight instruments

A time-of-flight instrument is a real-time method used to measure aerodynamic particle size and size distribution with high resolution and over a wide range of particle sizes. Such an instrument first uses a sharp contraction, which forces the aerosol particles to accelerate. The time interval for a particle to move between two narrowly focused laser beams is then recorded. Since larger particles have a higher inertia they accelerate more slowly. Therefore, the recorded time intervals can be used to calculate aerodynamic diameter once the instrument has been calibrated. Calibration is performed using monodisperse particles of known aerodynamic diameters. However, both agglomerated particles and particles with a density vastly different from 1000 kg/m^3 are not suited for measurements using such an instrument. In both cases the drag can differ significantly from that of calibrated particles with the same aerodynamic diameter, making the measurement unreliable. Also, coincidence errors occur if a second particle arrives between the laser beams before the first has left. This source of error increases when measuring higher particle concentrations. Lastly, commercially available time-of-flight instruments have a range of operation of particles between 0.5 and 20 μm, making

them unsuitable for measurements of nanoparticles.

2.3.3 Optical instruments

An optical particle counter (OPC) is an instrument that relies on the interaction between a particle and light to make non-invasive, real-time and in situ measurements. It is a pure optical instrument since it measures the intensity of the scattered light to deduce the particle size. The recorded signal is converted to particle size by the use of calibration curves from monodisperse, spherical particles with a known size and refractive index. Known limitations of optical particle counters are that the recorded signal is different for particles of different materials, and that it is not a monotonous function of particle size. As in the time-of-flight instrument, only one particle at a time can be present in the sensitive measuring volume in order to perform correct measurements. This may have to be achieved by diluting the aerosol. The particle size range covered is about the same as for time-of-flight instruments.

A condensation particle (or nucleus) counter (CPC) is simpler optical instrument that measures the number concentration of submicrometer aerosol particles [24]. In such an instrument, the aerosol continuously flows through a volume with supersaturated alcohol vapor, normally butanol. The aerosol is subsequently cooled either by adiabatic expansion or by passing through a chilled tube. The aerosol particles will thus grow in size due to heterogeneous nucleation, i.e., vapor condensing upon them. All particles are exposed to same level of supersaturation, which makes them grow to droplets of about 10 μm in diameter. The droplets can be counted by letting them pass a focused laser beam whereby it is possible to detect a change in transmitted light. The signal is easily converted to particle number concentration since each particle grows to one droplet. A CPC is suited for concentrations between $10^{-4} - 10^{7}$ cm^{-3} and particle sizes down to approximately 3 nm. A CPC is however only a counting instrument, and it requires a condensing vapor, normally alcohol, to function.

2.3.4 Electron imaging

Electron microscopy is a powerful tool for imaging aerosol nanoparticles. It makes use of a beam of electrons for precise measurements of the size and shape of individual particles. Transmission electron microscopy (TEM) and scanning electron microscopy (SEM) are two principally different types. Since both types make use of an electron beam to create images, a high-vacuum environment must be used
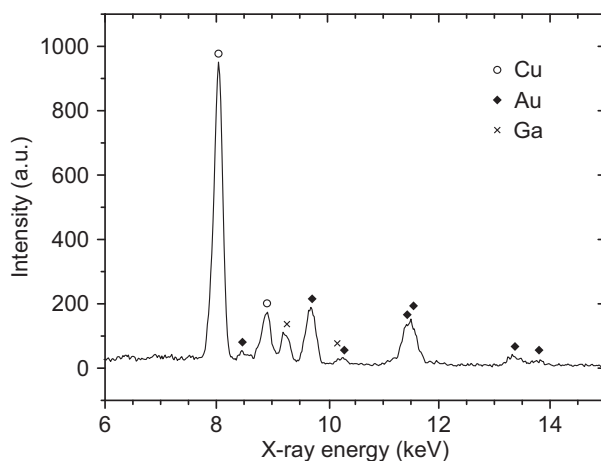
Figure 2.3: An XEDS spectrum taken of the particle shown in Fig. 2.4(a). Peaks emanating from Cu, Au, and Ga are identified.

in order to prevent scattering of the electron beam by gas molecules. Investigations are therefore limited to particles that can withstand the possible heating of the electron beam and do not evaporate in the high vacuum.

An X-ray induced energy dispersive spectrometer (XEDS) is usually mounted to an electron microscope, and can be used for elemental analysis of individual particles. This is performed by detecting the characteristic photons emitted from the particle upon electron beam irradiation. In Fig. 2.3, an example of a spectrum recorded by an XEDS is shown, here for the particle shown in Fig. 2.4. The detected peaks are identified in the spectrum as emanating from Au, Ga, and Cu, respectively. Au and Ga comes from the particle, and Cu comes from the copper grid.

Transmission electron microscopy

TEM images are created by letting a beam of electrons be transmitted through the sample thereby projecting a two-dimensional silhouette image, much like in a transmission light microscope. Thin samples are required in order to suppress electron beam attenuation . TEM is therefore best suited for particles smaller than 500 nm in diameter. Relevant to this thesis work, particles were deposited onto fine mesh copper grids with a thin carbon film covering the screen openings. High resolution TEM has atomic resolution, offering the possibility to study the
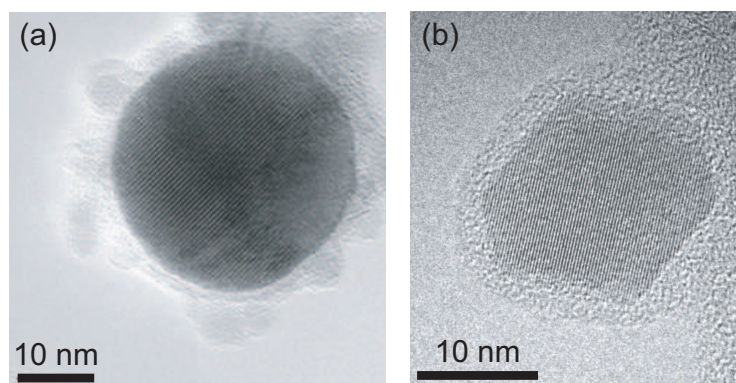
Figure 2.4: Examples of TEM images. (a) A nanoparticle composed of Au and Ga, as analyzed by XEDS shown in Fig. 2.3. The particle is created with the method presented in Paper III. The core consists mainly of Au, and the smaller particles attached to the core consists of pure Ga. (b) An iron-containing nanoparticle created with the method presented in Paper V.

morphology and crystalline phase of individual nanoparticles. Two examples of TEM images of nanoparticles are shown in Fig. 2.4. The method for producing compound nanoparticles of Au and Ga is presented in Paper III. The method for producing iron-containing nanoparticles is presented in Paper V.

Scanning electron microscopy

In an SEM, images are created by detecting the secondary electrons created as a focused electron beam is scanned over the surface of the sample. Different materials will result in different amounts of secondary electrons. It is therefore possible to distinguish for instance particles of one material from the substrate due to difference in contrast. The resulting images will have a three-dimensional appearance, since higher points on the sample are closer to the detector and more secondary electrons are collected from these points than the lower ones. This can be enhanced by tilting the sample in relation to the electron beam source, thereby creating realistic shadows. SEM is suitable for accurate measurements of substrate surface characteristics such as particle coverage, since it can image the sample surface well. Measurements of size and shape of individual nanoparticles is better performed by a TEM due to its higher resolution. Examples of SEM images are presented in Fig. 3.2.

2.4   Particle deposition

The most important deposition processes for nanoparticles are by diffusion, thermophoresis and electrostatic forces. The forces involved in these processes are all stronger than the gravitational force, which otherwise causes larger particles to deposit by sedimentation. Furthermore, the smaller the particle, the lower the inertia. This makes deposition via impaction less likely for nanoparticles.

2.4.1   Deposition by diffusion

Diffusive deposition occurs as a result of the randomness in the path traveled by nanoparticles, caused by collisions with the gas molecules. When close enough to a surface, the particle will adhere to it. At the surface, the number concentration of particles in the gas-phase is zero. This creates a concentration gradient out to the bulk aerosol, which drives a continuous diffusion of particles to the surface. For example, particles passing through a tube are lost to the walls due to diffusion. In the case of fully developed laminar flow, the penetration P (i.e., the fraction of entering particles that exit) can be calculated by the use of the dimensionless deposition parameter, μ,

$$\mu = \frac{DL}{Q} \tag{2.7}$$

where D is the particle diffusion coefficient, L is the length of the tube, and Q is the volumetric flow rate through it. The penetration is then given by simple analytical functions of μ. In Paper II this concept is adapted for calculating the diffusional losses inside a DMA.

A special case of diffusion is thermophoresis, a phenomenon which appears as a result of a temperature gradient in a gas. This gradient will cause an aerosol particle to move in the direction of decreasing temperature. Particles are transported as a result of a greater transfer of momentum from the colliding gas molecules on the hot side of the particles than on the cold one. Instruments that exploit this phenomenon to collect particles are called thermal precipitators. In Paper III, thermophoretic deposition was used to collect particles onto TEM grids placed at the outlet of a tube furnace.

2.4.2 Deposition by electrostatic forces

The work in this thesis primarily used deposition of charged particles by electrostatic forces as the method for collecting nanoparticles. This was a logical choice to make use of these forces since all of the particles selected by a DMA are charged. Particles were deposited with a so called electrostatic precipitator (ESP), which uses an electric field to attract the particles. The instrument consists of a grounded deposition chamber with a collector plate inside it connected to high voltage. The flow of charged particles enters the chamber via an inlet and is then directed towards the plate, which is placed perpendicular to the flow direction. Substrates (e.g., intended for electron microscope analysis of particles) can be placed on the conductive plate. Particle deposition occurs when the high voltage is applied. All particles charged with polarity opposite to the collector plate are deposited. Any other particles will simply follow the gas stream lines out of the chamber. Particles are collected inside a circular deposition spot. The spot size is determined by the electrical mobility of the particles. Larger particles, having a lower electrical mobility, will be deposited in a larger spot than smaller particles. In a well constructed ESP the particle surface density is uniform within the spot, and zero elsewhere [25].

The two main adhesive forces for nanoparticles are van der Waals force and electrostatic force. The stronger of these two is van der Waals force, which arises as a consequence of fluctuating electric dipole moments. The random movement of electrons in an electrically neutral material creates instantaneous areas of concentrated charge, or dipoles. These dipoles fluctuate over time and may induce complementary mirror dipoles in a neighboring material. This produces a strong attractive force, extending over very short distances in comparison to particle dimensions.

Charged particles induce an equal and opposite charge in the surface, which give rise to an attractive electrostatic force. For two charged particles (point charges), this force is inversely proportional to the square of the charge separation distance, as described by Coulomb's law. After initial contact between a particle and a surface by either or both of the above forces, a gradual deformation of the two contact areas occurs, leading to a decreasing separation distance. This process is halted when the attractive forces balance the forces resisting deformation. Once a particle is stuck to a surface, it does not move unless acted on by a much stronger force, e.g., mechanical manipulation with an atomic force microscope [26].

Martin Karlsson

2.4.3 Electrometer

An aerosol electrometer offers a simple and accurate method to measure the number concentration of charged nanoparticles on-line. The sample aerosol flow is passed through a filter, in which the particles are collected. The filter is insulated and connected to an ampere meter. The measured current, which is by definition the number of charges per unit time, can be converted to charges per unit volume since the sample flow rate is known. For nanoparticles with a Boltzmann equilibrium charge distribution, this charge concentration is in practice the particle number concentration, since almost all these nanoparticles are singly charged (cf. Table 2.1). Compared to a CPC, an electrometer is simpler in both construction and operation, especially since it does not consume alcohol [27].

Chapter 3

Aerosol nanoparticle formation

Aerosol nanoparticle formation routes in material synthesis can be categorized in two ways depending on the method of formation. In the first formation method, droplet-to-particle, a liquid is sprayed to form droplets, which dry to form particles. In section 3.1, different droplet-to-particle techniques relevant to this thesis work will be described. In the second formation method, gas-to-particle, the particles are formed from individual atoms or molecules in a gas colliding to form small clusters, a process known as homogeneous nucleation. In section 3.2, relevant gas-to-particle processes will be presented in detail.

What characteristics would an ideal aerosol generator have? Most important, it would have a constant and reproducible output of aerosol particles whose size and concentration is easily controlled. The particles should be monodisperse, i.e., with a size distribution having a geometric standard deviation of less than 1.2. Further, they should be spherical, stable and uncharged. Since perfectly ideal generators do not exist, there is always a trade-off between these different characteristics. The choice of generator among the available ones therefore depends on the intended application, and its specifications. For instance, in almost all applications the most important feature is to have a constant output of particles over time, but less important that they are uncharged.

3.1 Droplet-to-particle methods

One of the simplest way to generate aerosol particles is by different spraying methods, a few of them will be described in this section. The general principle for all of them is the continuous break-up of a liquid into droplets suspended in a gas, a process known as atomization. The liquid can either be a solution (e.g., salt dissolved in water) or a colloid suspension. The solid aerosol particles are created as the droplets evaporate, leaving a dry residue.

An important calibration technique for different sizing instruments is to atomize monodisperse polystyrene latex (PSL) spheres, commercially available in a size range from 0.01 to 30 μm.

Common to all droplet-to-particle methods described here are that the droplets (and thus the particles) produced are likely to be moderately charged, for which neutralization might be needed. The charging comes from the fact that there are almost always charges present on the surface of the liquid to be atomized, which are transferred to the droplets. The charge remains on the particles after drying. In the case of electrospray however, this charging ability is exploited to enhance the droplet production.

3.1.1 Atomizers

Atomizers are instruments that generate particles via atomization of a liquid. The simplest type is the pressure atomizer, which uses pressurized gas to convert the liquid into droplets. The droplets, and hence the particles, produced by an atomizer are coarse, thus making it only interesting for those applications where producing small particles is not important, e.g., spraying paint, perfumes or pesticides. When smaller particles are wanted, a nebulizer can be used instead, which is a type of atomizer from which only the smallest droplets are allowed to escape. In a nebulizer, the pressurized gas enters via an orifice at a high velocity past the liquid inlet. The pressure drop formed at the exit nozzle draws a thin liquid filament, which is accelerated into the exiting gas flow until it breaks into droplets. The larger spray droplets are removed by impaction within the device, and drained back to the liquid reservoir. This causes only the smallest droplets to escape, but it also makes the solution used more concentrated. The consequence of this is that the sizes of the produced particles will increase with time. The resulting size distribution from a nebulizer is broad. By changing the flow rates involved, the distribution can be shifted. In Paper I and II, a nebulizer containing sodium chloride solution was used to generate particles between 13 and 100 nm.

Monodisperse droplets can be produced with an instrument called vibrating orifice aerosol generator (VOAG). In such an instrument, the liquid is driven through an orifice coupled to a piezoelectric crystal, which is used to make the orifice oscillate along its axis. The oscillations causes the liquid to break into equally sized droplets, and the size can be calculated directly from the liquid feed rate and the frequency of the oscillations. The diameter of the generated droplets range from 15 to 100 μm. This aerosol generator was not used during the course of this thesis work.

3.1.2 Electrospray principles

An electrospray refers to the atomization of a conductive liquid through the Coulombic interaction of charges on the liquid surface and the applied electric field [28]. This interaction results in both the acceleration of the liquid and the subsequent disruption into droplets. This type of atomization is termed as electrohydrodynamic since it involves electrical forces exerted on a liquid that is moving during the atomization. The method has been used for electrospraying different colloidal solutions in combination with a DMA [29] or a chemical vapor deposition reactor [30].

The principle of operation of an electrospray is schematically shown in Fig. 3.1. A liquid is fed slowly through a hollow needle, or capillary. The feed is maintained either by a stable differential pressure that causes the solution to be pushed through the capillary or by means of a constant output syringe pump. The needle is connected to a high-voltage supply, which is used to establish an electric potential between the needle and a grounded coaxial ring placed a few centimeters away from it. A strong electrostatic field can thereby be exerted at the capillary exit, pulling the charged solution out of the capillary. As the liquid reaches the end of the capillary, the electric field induces a surface charge, which produces forces that cause the liquid to disperse into a fine spray of highly charged primary droplets from the needle tip. This jet of generated droplets is transported by a sheath gas flow, normally a mixture of air and CO_2, surrounding the needle. CO_2 is used for its ability to suppress electrical breakdown. To reduce the charge on each primary droplet, a radioactive ionizer is used. It is important that this neutralization is performed quickly after the droplet generation, since the droplets start to evaporate, leading to a decrease in surface area, hence an increase in surface charge density. If the surface charge density becomes too large, the Coulombic repulsive forces on the droplet will cause Rayleigh disintegration. Since this creates a large
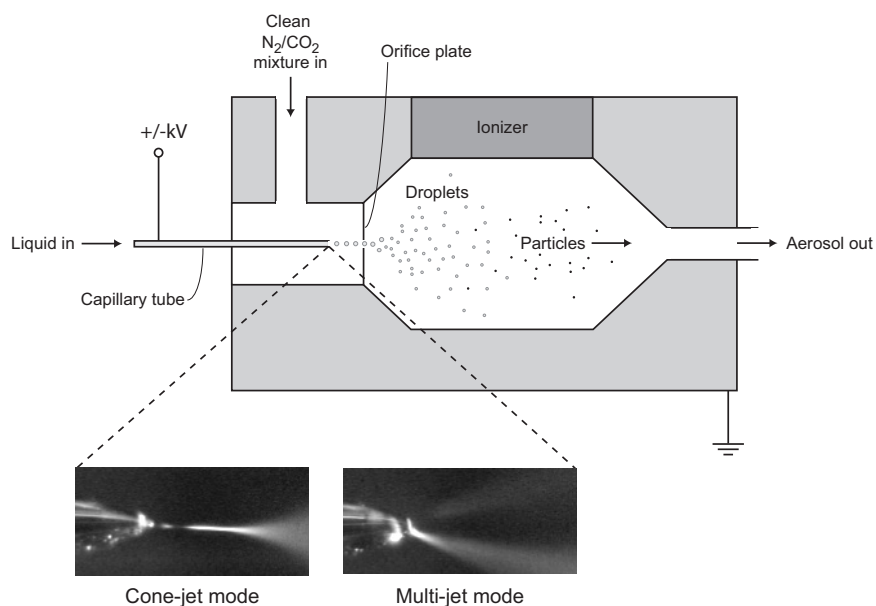
Figure 3.1: Schematic diagram of the electrospray with magnifications of the capillary needle tip showing two different spraying modes.

number of smaller droplets, it results in a less monodisperse aerosol. After neutralization, particle generation occurs as the liquid in the droplets evaporate leaving an aerosol particle. For instance, if a salt solution is used to generate an aerosol, the salt concentration can be varied to generate different particle diameters.

By balancing the liquid feed rate, the applied voltage and the involved gas flow rates, it is possible to get a dynamic equilibrium, creating a jet of droplets due to continuous break-up of the liquid at the tip. The most frequently used mode is the cone-jet mode, in which a stable so called Taylor cone is formed of the liquid meniscus at the capillary exit, cf. Fig. 3.1. This is the mode most efficient to produce a large number of droplets at a high rate. Multi-jet mode is also shown in Fig. 3.1. This mode is achieved when the applied voltage is too high, causing several droplet jets to be formed.

3.1.3 Electrospray experiments

An Electrospray Aerosol Generator (EAG, model 3480, TSI Inc.) was used to investigate the possibility to generate an aerosol by electrospraying a monodisperse

colloid suspension. The idea was to capture at the most one colloid particle per generated droplet.

Experimental

The EAG was operated with a N_2/CO_2 gas mixture. During the experiments, the EAG was run with a N_2 gas flow of 1.0 l/min, a CO_2 gas flow of 0.1 l/min, a high-voltage of 2.70 kV, and a capillary pressure drop of 25.5 kPa. A stable Taylor cone was achieved for these parameter values. With an inner diameter of 30 μm of the capillary, the liquid flow rate was calculated to 0.14 μl/min [31]. The generated particles were collected onto Si substrates using an electrostatic precipitator, with collection voltage of –6 kV. The ESP was placed horizontally at the outlet of the EAG, and substrates were fixed using conductive carbon tape.

Suspensions with Au colloid particles of two different sizes were used, 20 nm and 60 nm (purchased from British Biocell International), and Ag colloid particles of 80 nm (prepared by H. Xu [32]). The effects of deposition time and solution dilution ratio were both investigated, and two samples were prepared for 60 nm Au and 20 nm Au, respectively. For 60 nm, an undiluted colloid solution was used for generating particles under 1.5 h (case *A*) and 16 h (case *B*), respectively. For 20 nm Au, particles were deposited for 1 hour, one with a undiluted colloid solution (case *C*) and one with a 1:1 mixture with ultra pure H_2O (case *D*). Ag colloid particles were collected for 1 h.

A small droplet of undiluted colloid solution of 60 nm Au particles were put on a silicon substrate and blow-dried with N_2 gas. The sample was imaged by SEM and used as a reference to the samples of electrosprayed particles.

Results and discussion

Representative SEM images of the four cases of electrosprayed Au colloids are presented in Fig. 3.2, all of same magnification. The Au particles are visible as bright spots, and correspond well with the expected values of 20 nm and 60 nm, respectively. It should however be stated, that 20 nm is close to the resolution limit of the SEM. In the case of Ag, SEM images showed single particles well separated and in sizes corresponding to the as prepared colloid solution, 80 nm.

From all of the images it is clearly visible that it is possible to generate single particles. However, there is also a huge amount of other, smaller particles present in all of the images, unfortunately not clearly visible in Fig. 3.2. These particles are believed to emanate from droplets not containing any colloid particle(s). A
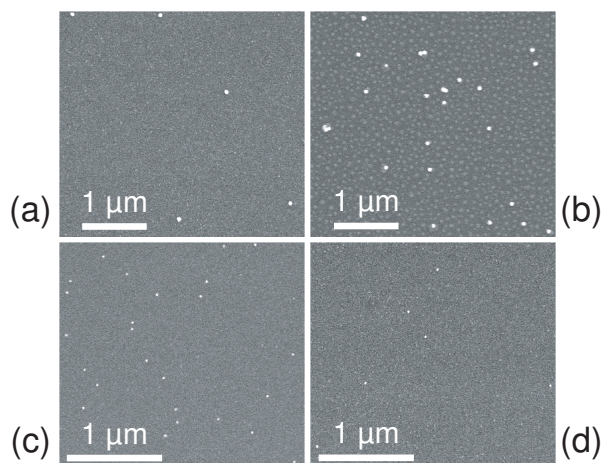
Figure 3.2: Examples of representative SEM images of electrosprayed Au colloid particles, (a) and (b) showing 60 nm Au, and (c) and (d) showing 20 nm Au. See text for a detailed discussion.

dry residue is left upon drying, probably consisting of salts or other dissolved matter in the solution. Imaging these particles individually with the SEM was not possible, since they were degraded by the electron beam.

Comparing Fig. 3.2(a) and (b), longer deposition time leads to a higher surface density. The multiple particles present in Fig. 3.2(b) are most probably a result of droplets containing more than one particle rather than particles depositing close to each other, since only particles with positive polarity were deposited. No multiple particles were found in the case represented by Fig. 3.2(a). The surface densities for case A and B were measured to be 0.10 μm^{-2} and 1.4 μm^{-2}, respectively (multiple particles were counted as emanating from one generated droplet). This corresponds well to the expected factor of 11, calculated from the different deposition times.

Comparing Fig. 3.2(c) and (d), a diluted colloid solution apparently leads to a lower surface density. The surface densities for case C and D were measured (from an ensemble of images) to be 2.5 μm^{-2} and 0.6 μm^{-2}, respectively. The factor 4 (and not the expected 2) in surface density between these two cases could be explained by different, non-comparable, electrospray modes. Taylor cones were achieved in both of the cases, but the cone in case D was probably creating droplets in a rate lower than half of the rate produced by the cone in case C. Solutions with higher water-to-colloid dilutions were tested, but stable Taylor
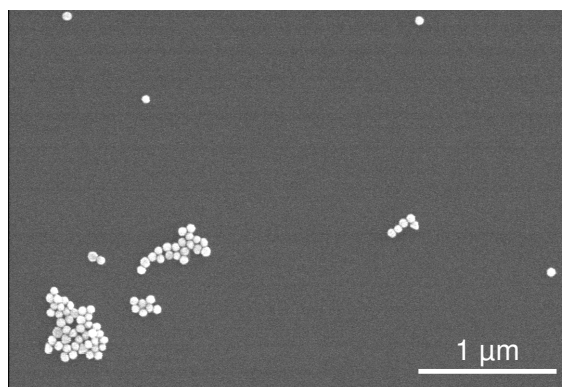
Figure 3.3: SEM image of the colloid reference sample. A droplet of undiluted solution of 60 nm Au colloid particles was put on a substrate for drying.

cones could not be accomplished.

Shown in Fig. 3.3 is the reference sample of 60 nm Au colloid particles. Single particles are present, although agglomerates are dominating. In comparison to Fig. 3.2, it can thus be concluded that it is possible to achieve controlled deposition of colloid particles using an electrospray.

Conclusions

To summarize, these experiments showed it possible to generate single aerosol particles from a colloidal suspension by the use of an electrospray method. The particle surface density could be controlled by varying the deposition time and/or the dilution ratio, respectively. Multiple particles are only present at very long deposition times. The method appears to be independent of colloid particle material. This result is very important, since it implies that a method once developed for generating aerosol particles of one kind is easily adapted to particles of a different kind.

3.2 Gas-to-particle methods

There are a variety of different nanoparticle generation methods that are based on the concept of evaporation and condensation. This type of generation process is an example of a gas-to-particle conversion. In common, a supersaturated vapor is first created by evaporation, which then initiate the formation of small nuclei,

or primary particles, by condensation. The main difference between different evaporation/condensation production methods is the way to evaporate the material. In this section, common basic concepts for the different generation methods are described. The method used throughout this thesis work, which includes the evaporation from a metal, is presented in detail in the next section, 4.1.

We follow here the basic definitions found in different aerosol standard textbooks [1, 2, 33]. The term *nucleation* is used to describe the initial formation of stable, chemically homogeneous metal clusters from a supersaturated vapor. *Condensation* is the process of cluster growth via collisions with vapor phase metal atoms (monomers). *Coagulation* is the process of cluster growth via collisions between metal clusters, followed by coalescence (sintering) of the clusters (coagulation was originally referring to hydrosols, but is now also valid for aerosols). Coagulation occurs without requiring a supersaturation, and is a one-way growth process resulting in an increase in particle size and a decrease in aerosol number concentration. For solid particles, coagulation is often called *agglomeration*, and the resulting, unsintered, particles are phrased as agglomerates. The *partial pressure* of a vapor in a mixture of gases is defined as the pressure that would be exerted by that vapor if it were to occupy all by itself the entire volume that is occupied by the gas mixture. Expressed as a fraction of the total pressure, this pressure is describing the fractional concentration of vapor.

3.2.1   Particle generation

With an evaporation/condensation method, primary particles are formed by homogeneous nucleation, a process in which critical clusters are formed without the assistance of a condensation nuclei of a different material and/or phase, as in heterogeneous nucleation. Evaporation/condensation methods are therefore well suited for production of single-component particles, since the level of purity can be chosen arbitrarily. However, to form particles via homogeneous nucleation a high level of supersaturation is needed, due to the so called Kelvin effect.

The Kelvin effect describes the increase in saturation vapor for pure materials due to decreasing droplet diameter. The saturation vapor pressure (or simply: vapor pressure), p_s, is defined as the partial pressure required to maintain mass equilibrium—that is, no net evaporation or condensation—for a flat liquid surface (mathematically, this is a droplet with an infinite diameter). However, for a liquid droplet having a sharply curved surface, the partial pressure required to maintain mass equilibrium, p_d, is greater than over a flat surface for a given tem-

perature T. The curvature causes molecules to easily leave the droplet, hence a greater partial pressure is needed to maintain mass equilibrium. This is the Kelvin effect, and is described by in terms of the saturation ratio, S_R

$$S_R = \frac{p_d}{p_s} = \exp\left(\frac{4\gamma M}{\rho R T d^*}\right) \tag{3.1}$$

Here, R is the gas constant, γ, M, and ρ are, respectively, the surface tension, molecular weight, and density of the liquid droplet with the diameter d^*. In Fig. 3.4, Eq. 3.1 is plotted for Au at 1850°C. A droplet with diameter d^* will neither grow nor evaporate at a constant pressure p_d, hence Eq. 3.1 describes the boundary between evaporation and condensation. The region above the curve in Fig. 3.4 is a growth region and that below, an evaporation region. As can be seen, S_R increases dramatically for very small particles. The implication of this would be that an infinite S_R would be required to nucleate primary particles from a gas! Fortunately, molecular clusters are always present even in an unsaturated vapor as a result of collisions among the atoms. The attractive interatomic forces are weak, which means that the clusters are highly instable, making them to continuously break apart. In a supersaturated vapor, however, these clusters increase in number concentration and pass through the critical size d^* by attachment of single atoms. The critical clusters can be regarded as a form of condensation nuclei, which grow into primary particles via subsequent condensation. These in turn will increase in size by further condensation, and particle agglomeration. As a result, the supersaturation in the gas will decrease, unless there is a continuous flux of atoms maintaining the supersaturation.

The particle formation rate, I, is expressed as particles per unit volume of gas per unit time. Assuming I is independent of cluster size, it can be described by the following expression [33]:

$$I = 2\left[\frac{p_1}{(2\pi m_1 k_B T)^{1/2}}\right](n_1 v_1^{2/3})\left[\frac{\gamma v_1^{2/3}}{k_B T}\right]^{1/2}\exp\left[-\frac{16\pi\gamma^3 v_1^2}{3(k_B T)^3(\ln S)^2}\right] \tag{3.2}$$

where p_1 is the partial pressure of condensing monomers of mass m_1, number concentration n_1, and volume v_1. The first term in brackets is the monomer flux (atoms per unit area per unit time) and the second is proportional to the monomer surface area per unit volume of gas. The term $\gamma v_m^{2/3}/k_B T$ is dimensionless. In Fig. 3.5, the particle formation rate is plotted for Au vapor at 1550°C, 1700°C and 1850°C as a function of saturation ratio. Necessary data are taken from Refs.
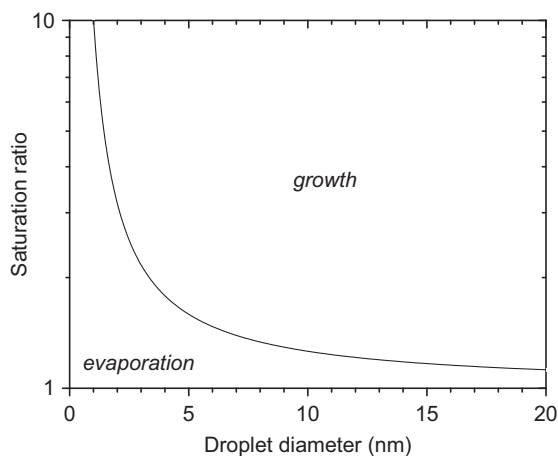
Figure 3.4: Saturation ratio as a function of particle diameter for pure gold at 1850°C. The region above the curve is a growth region and that below, an evaporation region.

[34] and [35]. p_1 is taken as $p_s(T)$, m_1 is calculated by dividing the molecular weight of Au with Avogadro's number, N_A, and v_1 is calculated by dividing m_1 with the bulk density of Au. The monomer number concentration is calculated from the ideal gas law

$$n_1 = \frac{p_s}{k_B T} \tag{3.3}$$

As seen in Fig. 3.5, the particle formation rate is strongly dependent on temperature. Also, homogeneous nucleation is nearly an all-or-nothing phenomenon; a small change in S_R results in a huge difference in I. The critical saturation ratio, S^*, is defined as when particle formation rate equals unity. S^* is approximately 13 for 1750°C, and 8 for 1850°C. For 1064°C (melting point of Au [34]), S^* equals approximately 360, implying that particle formation by homogeneous nucleation at that temperature is practically impossible.

If a fine mesh grid made of Au is used instead of a flat surface, particle formation is possible at a much lower temperature [36]. In this case, atoms are probably more easily evaporated due to the small curvature of the thin mesh wires, and the larger surface area of the mesh as compared to a flat surface.
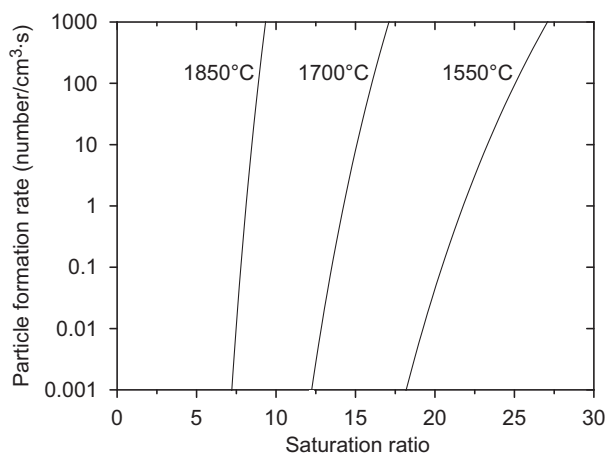
Figure 3.5: Particle formation rate by homogeneous nucleation for Au at three different temperatures as a function of saturation ratio.

3.2.2 Sintering

Particles formed by evaporation/condensation methods grow by condensation driven by the vapor supersaturation. As the vapor gets consumed and supersaturation ceases, the particles will start to grow by coagulation processes. This growth caused by collisions leads to fractal-like particles, or agglomerates, which are composed of primary particles bonded together. In most applications, particles of spherical shape are preferred. Therefore, a compacting step is frequently performed to reshape the particles. This is normally done by sintering, in which the particles are fused together at a temperature below the particle melting point. Sintering is a irreversible thermodynamic process, which changes unstable agglomerates into stable compact particles.

Sintering occurs as a consequence of material transport in the form of atomic diffusion, leading to stronger bonding between the particles as the pores are gradually eliminated between them. The rate of sintering is determined by the rate of diffusion, which is dependent on the temperature and the path of diffusion. For nanoparticles, three different diffusion paths are important: diffusion on the particle surface, along grain boundaries, and volume (or bulk) diffusion. Surface diffusion is the quickest due to minimum constraints of the diffusing atoms, whereas volume diffusion is the slowest since it involves the movement of atoms from one lattice position to another. The relative importance of these diffusion

paths is dependent on material and varies with temperature. However, the net diffusion rate includes contributions from all three processes.

Depending on the bond strength between neighboring primary particles in an agglomerate, the process of sintering will be different. For strongly bonded particles, the main mechanism is coalescence, which causes the particles to become fused together [37]. This mechanism is understood by the aforementioned discussion of diffusion, and is initiated by a neck formation between two particles. On the other hand, if the primary particles are loosely bonded, particle rearrangement are more likely to occur [38]. The particles tend to collapse and become more compact as the temperature is increased, as in the case of Ag [39].

3.2.3   Alloying

Alloy aerosol nanoparticles, or nanoalloys, are compound particles with a specific composition of two (or more) elements. These can be produced via a two-step evaporation process. The first step includes formation of nanoparticles of one material via evaporation/condensation, size classification using a DMA, and sintering of the produced particles. The second step involves controlled condensation of another material upon the sintered particles. Compound particles are formed by heterogenous nucleation with the first particles acting as condensation nuclei when passing through a region of supersaturated vapor of the other material. The level of supersaturation required is lower as compared to homogeneous nucleation. A second sintering step is not needed for particles reshaping, since the compound particles are not agglomerates. However, sintering can be necessary for internal rearrangement purposes.

3.2.4   Precursor thermal decomposition

A supersaturated vapor of a material can also be accomplished by pyrolysis of a gas-phase precursor. Pyrolysis is defined as the decomposition of a compound as a result of subjection to very high temperatures [40]. The process is also known as thermal decomposition, or simply cracking. In such a method, a precursor containing the material of interest is exposed to a temperature for which it decomposes, yielding a condensable material. The vapor pressure is often low at the cracking temperature, resulting in a high level of supersaturation. Particles are formed according to the processes described in section 3.2.1. This method is suitable for materials that require high temperatures for creating supersaturation in an ordinary evaporation/condensation method.

The precursor can be cracked inside a hot-wall tubular reactor, in which the carrier gas containing the precursor is heated. This method has been employed for the production of W nanoparticles from $W(CO)_6$ [41], TiO_2 from titanium tetraisopropoxide [42], and copper oxide nanoparticles from copper acetylacetonate [43]. The precursor can also be dissociated by laser pyrolysis, a method described in the next section.

3.2.5 Alternative supersaturation techniques

In the previous sections, methods to produce a supersaturated vapor for particle formation most relevant to this thesis work have been described. There are of course a variety of other, complementary methods, which utilize different techniques for establishing vapor supersaturation. Some of them will be briefly described in the following.

Laser techniques

Laser can be used to initiate chemical reactions that result in nanoparticle formation. Three major types can be identified: ablation, pyrolysis, and photolysis.

In ablation, the energy of a pulsed laser beam can be used to locally heat a target sample, which undergo vaporization due to the energetic plasma formed above it. A large amount of atoms are released per pulse, which can form particles by homogeneous nucleation. However, fragments of solid or liquid material are also released, or ablated, hence the method is referred to as laser ablation [44]. This method has been used for production of, e.g., Si nanoparticles by ablation of crystalline silicon substrates [45, 46] and nanoparticles by ablation of micrometer-sized metal particles [47].

In laser pyrolysis, a precursor is heated rapidly with an IR laser, e.g., a continuous-wave (cw) CO_2 laser [48]. By absorption of the laser beam energy the precursor molecules are heated selectively, and the carrier gas is only heated indirectly via collisions of reactant molecules. For example, the method has been used for formation of Fe nanoparticles from $Fe(CO)_5$ [49, 50], Si nanoparticles from SiH_4 [48, 51], and carbon-based nanoparticles from hydrocarbons [52].

In laser photolysis, the laser radiation is used to induce photochemical decomposition of the precursor. The wavelength of the laser light is chosen to correspond with the energy of the bond to be dissociated. For example, photolytic dissociation of ferrocene has been used for the formation of iron-containing nanoparticles [53], and UF_5 nanoparticles produced from laser photolysis of gaseous UF_6 [54].

The method is advantageous in that the size distribution of the particles formed can be controlled by the laser parameters, such as repetition rate, pulse energy, and beam diameter [55].

Arc evaporation

Evaporation of a metal for nanoparticle formation can be achieved by establishing a d.c. spark discharge between two electrodes. The spark creates a plasma, and the the source metal is evaporated and/or ablated due to the rapid increase in temperature. Particles are formed at high rates, for instance Si nanoparticles [56] and metal nanoparticles [57].

Closely related is the exploding wire technique, in which the wire material is completely evaporated in a chamber filled with an inert gas. The technique has for instance been used for synthesizing crystalline GaAs nanoparticles from a GaAs wire [58].

Flame and plasma reactors

Condensable monomers for particle formation can also be generated by chemical reactions of precursors in diffusion or premixed flames [59]. Flame reactors provide a simple and inexpensive particle generation method easy to scale up, however it yields agglomerated oxide particles with broad size distributions. As examples TiO_2, SnO_2, and SiO_2 nanoparticles have been produced by oxidation of their halide vapors in electrically assisted hydrocarbon flames [60] and in premixed flat flames [61]. The precursor can also be delivered in the form of droplet, a method known as flame spray pyrolysis [62].

In a plasma reactor, the reactive components are ionized and dissociated in a plasma. The plasma can be thermal, of which there are different generation types [63], or it can be microwave-generated [64, 65].

Chapter 4

Aerosol nanoparticle generator

For the production of aerosol nanoparticles during this thesis work, a versatile generator[1] set-up based on the concept of evaporation/condensation was employed. It includes tubular furnaces and DMAs, as schematically depicted in Fig. 4.1. The generator consists of (*i*) a first tube reactor used for particle formation, (*ii*) a first DMA, (*iii*) a second furnace used for sintering, (*iv*) a third furnace for optional condensation, (*v*) a second DMA, and (*vi*) an electrostatic precipitator and an electrometer. The system is interconnected with 1/4" stainless steel tubing, with Swagelok connections. During a run, the system is held at atmospheric pressure, balanced by the high pressure source of ultra-pure nitrogen gas and the low pressure sink in the form of a rotary vacuum pump. Normally, a volumetric flow of 1.68 ℓ/min ultra-pure particle-free nitrogen gas was continuously fed through the system, and the DMAs were run with a sheath nitrogen gas flow of 10 ℓ/min.

Particle formation

The first tube furnace was used for the creation of nanoparticles. Two types of resistively heated, hot-wall tube furnaces were employed, depending on creation method.

For the production of Au nanoparticles [66], a high-temperature furnace capable of reaching 1950°C was used. This is a well-established generation method,

---

[1]The term generator refers here to the total experimental set-up.
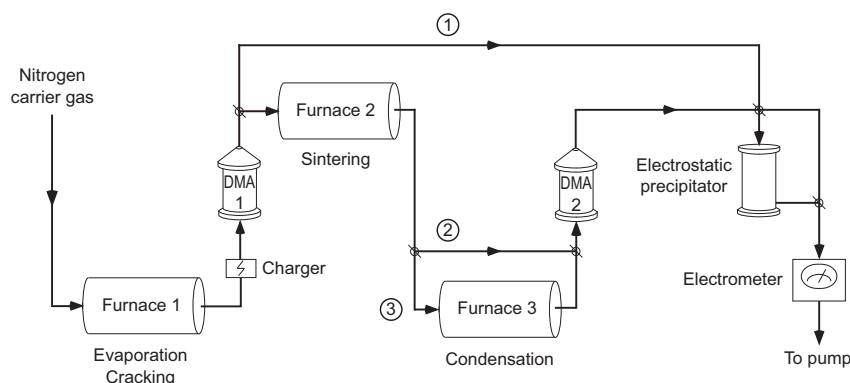
Figure 4.1: Schematic diagram of the aerosol nanoparticle generator.

and was first proposed by Scheibel and Porstendörfer for the production of Ag and NaCl nanoparticles [18]. A small crucible made of pyrolytic boron nitride (PBN) containing pieces of Au is put inside the graphite inner tube of the furnace. The tube is encompassed by a graphite meander, resistively heating the tube. The furnace temperature is controlled by a thermocouple mounted close to the graphite meander. The tube is surrounded by graphite insulation, which is covered by a metal housing. The interior of the furnace housing is purged with N_2 gas, whereas the outside is water-cooled. The ultra-pure N_2 carrier gas is flowed at a constant rate through the inner tube, carrying the evaporated material out of the hot region. As the gas cools down, the vapor becomes supersaturated and particles are formed according to the nucleation processes described in section 3.2.1. It is possible to shift the size distribution of the produced nanoparticles by changing the temperature of the furnace [66]. In Paper III, this furnace was used for the production of Au core particles.

The second furnace type is based on the same principle, but consists instead of a ceramic (Al_2O_3) inner tube. The tube is heated by a resistance coil and insulated by ceramic material. The furnace temperature is controlled by a thermocouple. This type of low-temperature furnace is capable of reaching $1200°C$, making it suitable for materials that require lower temperatures to reach the high vapor pressures needed for nanoparticle formation. The material to be evaporated is put in a small PBN crucible inside the tube, and particles are formed in a similar way as for the high-temperature furnace. Previous studies have made use of this for formation of Ag [67], Ga [68], and In [69] particles. In Paper IV, nanoparticles

of Ag, Ga, In, and Pb were formed with this type of furnace. The study aimed at investigating the flow pattern in the tube, and how the particle formation is affected. To allow for visual inspection of the depositions on the inside, quartz tubes were used.

Another method for creating gas supersaturation for particle formation is the thermal decomposition of a precursor, as described in the previous chapter. In Paper V, iron-containing nanoparticles were formed by thermal cracking of iron pentacarbonyl, $Fe(CO)_5$, in a low-temperature furnace. The $Fe(CO)_5$ was placed in a small evaporation cell connected to the carrier gas at a location upstream of the cracking furnace.

Size selection

Before entering the first DMA, the aerosol particles were brought to a known charge equilibrium by passing a bipolar charger containing a β-emitting radioactive source, ^{63}Ni. Since the probability of double charges is low for particles in the nanometer size range (cf. Table 2.1), the majority of particles selected by the DMA were singly charged. The particles often retained their charge throughout the process. Negative charging was normally chosen due to the higher charging probability (see Table 2.1), which effectively increases the particle yield through the DMA.

The aerosol flow (i.e., the carrier gas flow) was 1.68 ℓ/min and the sheath flow in the DMA was 10 ℓ/min. This gives a theoretical full width at half maximum, or resolution, of the selected mobility distribution of 1/6 (cf. Eq. 2.6). After DMA 1, the selected particles could be transported directly to the electrometer, via route nr. 1 in Fig. 4.1. By stepwise scanning the DMA 1 voltage and measuring the concentration with the electrometer, a size distribution of the produced particles in furnace 1 could be obtained.

Sintering

The particles selected in DMA 1 could also be directed towards a second furnace used for in-flight sintering. The furnace is of the same type as the low-temperature furnace described earlier. After the sintering furnace, the particles could be directed towards the second DMA (route nr. 2), allowing a measurement of the size distribution of the sintered particles to be obtained. The particle size was determined from the position of the peak in the mobility distribution. By making correlated measurements of the particle size as determined by DMA 2 as a func-

tion of sintering furnace temperature, a value of the compaction temperature, T_c, could be deduced. The compaction temperature represents the limit between agglomerated particles and fully sintered ones, in that particles exposed to temperatures greater than T_c will not compact further. For complete sintering of for example Au, the furnace had to be kept at 600°C [66], which is approximately 2/3 of the bulk melting point. In Paper VI, the sintering behavior of agglomerated aerosol nanoparticles of different materials are examined in relation to the compaction temperature.

Condensation

The sintered particles could also be directed towards a third low-temperature furnace, route nr. 3 in Fig. 4.1. This route offers the possibility for subsequent condensation of another material onto sintered core particles. For this purpose, a small crucible containing the material of interest is placed inside the tube of furnace 3. By heating the furnace, the vapor pressure over the surface of the material could be increased. Compound particles could be formed via heterogenous nucleation by letting the passing core particles act as condensation nuclei. In Paper III, this method was used to produce such binary nanoalloy particles composed of Au and Ga, and Au and In, respectively. Furthermore, nanoparticles of In and Se were also produced during the course of this thesis work [70].

Deposition

Independent on route, the particles could be transported to the electrostatic precipitator (ESP) for deposition onto substrates. By placing the substrates on the ESP collector plate and applying a high voltage, normally ±6 kV, charged particles were deposited within a spot. Examples of typical deposition spot diameters are 5 mm for 10 nm particles and 20 mm for 30 nm ones. The deposition time to reach a certain surface concentration is calculated from the aerosol particle number concentration.

A home-built aerosol electrometer was use to measure the number concentration of the charged particles. A typical current as measured by the electrometer was 500 fA, which corresponds to a number concentration of about 10^5 particles per cubic centimeter. This concentration corresponds to a deposition time of 1 min to achieve a substrate surface number concentration of 1 μm^{-2}.

The detection limit of the electrometer used in all of the experiments reported in this thesis was approximately 1 fA, corresponding to 10^4 singly charged parti-

cles per second. With a flow of 1.68 ℓ/min, this corresponds to a concentration of 300 particles per cubic centimeter, which is less than 1 % of the typical concentration of particles produced in the experiments.

Appendix

Derivation of transfer function for cylindrical DMA

The DMA transfer function is defined as the particle penetration as a function of the electrical mobility for a given voltage and flow setting. For a cylindrical DMA, the transfer function can be derived by considering the two perpendicular forces the particles entering the DMA will be affected by, the radial caused by the electric field and the axial caused by the gas flow. In Fig. A.1, the relevant parameters are defined (see also Fig. 2.1). Q_{sh} is the sheath gas flow rate, Q_a the inlet aerosol flow rate, Q_e the excess flow, Q_s is the sample flow leaving the DMA. The large arrow indicates the general gas flow in the DMA, defining the positive z-direction, and the r-direction is defined as positive from the center axis and outwards. The two perpendicular motions can be considered separately, resulting in two different expressions for the particle traveling times. The mean mobility of the particles leaving the DMA with the sample flow can thus be calculated by setting these two times equal.

Neglecting end effects, the radial electric field $E(r)$ as a function of the radius r for concentric cylinders (as the DMA classifier column) is given by

$$E(r) = \frac{U}{r \ln(r_2/r_1)} \tag{A.1}$$

where U is the applied voltage on the central electrode, r_1 and r_2 are the radii of the electrode rod and the outer cylinder, respectively (cf. Fig. A.1). Following the definition of the electrical mobility in Eq. 2.1, the (terminal) radial velocity $v_r(r)$ of a particle with mobility Z_p due to the electric field is

$$v_r(r) = -E(r)Z_p = \frac{dr}{dt} \Leftrightarrow dt = -\frac{dr}{E(r)Z_p}. \qquad (A.2)$$

Those particles traveling from r_A to r_D will have the mean mobility Z_p^* (note that the dashed line from A to D in Fig. A.1 is not representing a true particle trajectory, but acts as an eye guide-line). Combining Eqs. A.1 and A.2, the average radial traveling time t_r^* will be given by

$$t_r^* = -\int_{r_A}^{r_D} \frac{dr}{E(r)Z_p} = \frac{\ln(r_2/r_1)}{2UZ_p} \left(r_A^2 - r_D^2\right). \qquad (A.3)$$

Assuming the gas flow is fully laminar in the z-direction, the average axial velocity v_z^* is described by the particles traveling from r_A to r_D, and becomes

$$v_z^* = \frac{dz}{dt} = \frac{Q^*}{\pi \left(r_A^2 - r_D^2\right)} \qquad (A.4)$$

where Q^* is the average volumetric flow rate. This flow can be given as an expression of the appropriate flows (cf. Fig. A.1),

$$Q^* = Q_{sh} + \tfrac{1}{2}Q_a - \tfrac{1}{2}Q_s. \qquad (A.5)$$

The average axial traveling time t_z^* is given by

$$t_z = \frac{L}{v_z^*} \qquad (A.6)$$

which combined with Eq. A.4 becomes

$$t_z^* = \frac{\pi \left(r_A^2 - r_D^2\right)}{Q_{sh} + \frac{1}{2}\left(Q_a - Q_s\right)}. \qquad (A.7)$$

Since the two traveling times given by Eqs. A.3 and A.7 must be equal for the particles in the exiting flow, the mean mobility becomes

$$Z_p^* = \frac{\ln(r_2/r_1)}{2\pi UL} \left[Q_{sh} + \tfrac{1}{2}\left(Q_a - Q_s\right)\right]. \qquad (A.8)$$

There is of course a mobility range of the particles in the exiting flow due to the finite width of the exit slit. This range can be calculated in relation to the maximum ($Z_{p,max}$) and minimum ($Z_{p,min}$) mobility, which can both be derived in

an analogous way as described above. Particles traveling from r_2 to r_1 will have the maximum mobility and those traveling from r_B to r_C will have the minimum mobility. From Eq. A.8 it can be noted that the first factor is constant, and only the flow terms inside the brackets will change, hence the mobilities become

$$Z_{p,max} = \frac{\ln(r_2/r_1)}{2\pi UL}(Q_{sh} + Q_a) \qquad (A.9)$$

$$Z_{p,min} = \frac{\ln(r_2/r_1)}{2\pi UL}(Q_{sh} - Q_s) \qquad (A.10)$$

The total width of the mobility range ΔZ_p becomes

$$\Delta Z_p = \frac{\ln(r_2/r_1)}{2\pi UL}(Q_a + Q_s). \qquad (A.11)$$

Normally, a DMA is operated with symmetrical flows, i.e., $Q_{sh} = Q_e$ and $Q_a = Q_s$, thus the mean mobility can be calculated from Eq. A.8 using only the sheath gas flow rate Q_{sh}. The relative width then becomes

$$\frac{\Delta Z_p}{Z_p^*} = 2\frac{Q_a}{Q_{sh}}. \qquad (A.12)$$

and the transfer function becomes symmetric and triangular, as depicted in Fig. 2.2.
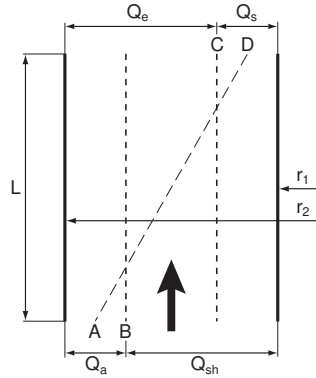
Figure A.1: Parameters of the cylindrical differential mobility analyzer relevant for the derivation of its transfer function. The dash dotted line represents the DMA center axis. Letters A – D refer to the text (the dashed line from A to D acts as an eye guide-line), and the large arrow indicates the direction of the general gas flow.

References

[1] W. C. Hinds, *Aerosol technology: Properties, behavior, and measurement of airborne particles* (Wiley, New York, 1999), 2nd edn.

[2] K. Willeke and P. A. Baron (Editors), *Aerosol measurement: principles, techniques, and applications* (Van Nostrand Reinhold, New York, 1993).

[3] F. E. Kruis, H. Fissan, and A. Peled, *Synthesis of nanoparticles in the gas phase for electronic, optical and magnetic applications – a review*, J. Aerosol Sci. **29**, 511–535 (1998).

[4] A. D. Yoffe, *Low-dimensional systems. quantum size effects and electronic properties of semiconductor microcrystallites (zero-dimensional systems) and some quasi-two-dimensional systems*, Adv Phys **42**, 173–266 (1993).

[5] A. P. Alivisatos, *Semiconductor clusters, nanocrystals, and quantum dots*, Science **271**, 933–937 (1996).

[6] V. L. Colvin, M. C. Schlamp, and A. P. Alivisatos, *Light-emitting diodes made from cadmium selenide nanocrystals and a semiconducting polymer*, Nature **370**, 354–357 (1994).

[7] M. K. Kennedy, F. E. Kruis, and H. Fissan, *Gas phase synthesis of size selected SnO_2 nanoparticles for gas sensor applications*, Mater. Sci. Forum **343-346**, 949–54 (2000).

[8] A. Mills and S. Le Hunte, *An overview of semiconductor photocatalysis*, J. Photoch. Photobio. A **108**, 1–35 (1997).

[9] A. I. Persson, B. J. Ohlsson, M. T. Björk, C. Thelander, M. H. Magnusson, K. Deppert, T. Sass, L. R. Wallenberg, and L. Samuelson, *Heterointerfaces in III-V semiconductor nanowhiskers*, IPRM 14th conference pp. 281–284 (2002).

[10] B. J. Ohlsson, M. T. Björk, A. I. Persson, C. Thelander, L. R. Wallenberg, M. H. Magnusson, K. Deppert, and L. Samuelson, *Growth and characterization of GaAs*

45

and InAs nano-whiskers and InAs/GaAs heterostructures, Physica E **13**, 1126–1130 (2002).

[11] E. O. Knutson and K. T. Whitby, *Aerosol classification by electric mobility: apparatus, theory, and applications*, J. Aerosol Sci. **6**, 443–451 (1975).

[12] H. M. ten Brink, A. Plomp, H. Spoelstra, and J. F. van de Vate, *A high-resolution electrical mobility aerosol spectrometer (MAS)*, J. Aerosol Sci. **14**, 589–597 (1983).

[13] W. Birmili, A. Wiedensohler, J. Heintzenberg, and K. Lehmann, *Atmospheric particle number size distribution in central Europe: statistical relations to air masses and meteorology*, J. Geophys. Res. **106**, 32 005–32 018 (2001).

[14] B. Y. H. Liu, D. Y. H. Pui, K. T. Whitby, D. B. Kittelson, Y. Kousaka, and R. L. McKenzie, *The aerosol mobility chromatograph: a new detector for sulfuric acid aerosols*, Atmos. Environ. **12**, 99–104 (1978).

[15] B. G. Martinsson, *Physical basis for a droplet aerosol analysing method*, J. Aerosol Sci. **27**, 997–1013 (1996).

[16] G. Frank, B. G. Martinsson, S. I. Cederfelt, O. H. Berg, E. Swietlicki, M. Wendisch, B. Yuskiewicz, J. Heintzenberg, A. Wiedensohler, D. Orsini, F. Stratmann, P. Laj, and L. Ricci, *Droplet formation and growth in polluted fogs*, Contr. To Atmos. Physics **71**, 65–85 (1998).

[17] B. Y. H. Liu and K. Lee, *An aerosol generator of high stability*, Am. Ind. Hyg. Assoc. J. **36**, 861–865 (1975).

[18] H. G. Scheibel and J. Porstendörfer, *Generation of monodisperse Ag- and NaCl-aerosols with particle diameters between 2 and 300 nm*, J. Aerosol Sci. **14**, 113–126 (1983).

[19] S.-H. Zhang, Y. Akutsu, L. M. Russell, R. C. Flagan, and J. H. Seinfeld, *Radial differential mobility analyzer*, Aerosol Sci. Technol. **23**, 357–372 (1995).

[20] H. Fissan, A. Pöcher, S. Neumann, D. Boulaud, and M. Pourpix, *Analytical and empirical transfer functions of a simplified spectromètre de mobilité electrique circulaire (SMEC) for nanoparticles*, J. Aerosol Sci. **29**, 289–293 (1998).

[21] A. Wiedensohler, *An approximation of the bipolar charge distribution for particles in the submicron size range*, J. Aerosol Sci. **19**, 387–389 (1988).

[22] M. R. Stolzenburg, *An ultrafine aerosol size distribution measuring system*, Ph.D. thesis, University of Minnesota (1988).

[23] P. Lee, D. R. Chen, and D. Y. H. Pui, *Experimental study of a nanoparticle virtual impactor*, J. Nanoparticle Res. **5**, 269–280 (2003).

[24] J. K. Agarwal and G. J. Sem, *Continuous flow, single-particle-counting condensation nucleus counter*, J. Aerosol Sci. **11**, 343–357 (1980).

[25] T. J. Krinke, K. Deppert, M. H. Magnusson, F. Schmidt, and H. Fissan, *Microscopic aspects of the deposition of nanoparticles from the gas phase*, J. Aerosol Sci. **33**, 1341–1359 (2002).

[26] T. Junno, K. Deppert, L. Montelius, and L. Samuelson, *Controlled manipulation of nanoparticles with an atomic force microscope*, Appl. Phys. Lett. **66**, 3627–3629 (1995).

[27] *Regeringens proposition 2000/01:20: Nationell handlingsplan för att förebygga alkoholskador* (Socialdepartementet, Faktablad nr. 13, nov. 2001, Artikelnr. S2001.035).

[28] J. Grace and J. Marijnissen, *Review of liquid atomization by electrical means*, J. Aerosol Sci. **25**, 1005–1019 (1994).

[29] I. W. Lenggoro, B. Xia, K. Okuyama, and J. F. De la Mora, *Sizing of colloidal nanoparticles by electrospray and differential mobility analyzer methods*, Langmuir **18**, 4584–4591 (2002).

[30] M. Danek, K. F. Jensen, C. B. Murray, and M. G. Bawendi, *Preparation of II-VI quantum dot composites by electrospray organometallic chemical vapor deposition*, J. Cryst. Growth **145**, 714–720 (1994).

[31] *Instruction manual (Rev. D) Electrospray Aerosol Generator, model 3480* (TSI Inc., Shoreview, MN, 2003).

[32] H. Xu and M. Käll, *Polarization-dependent surface-enhanced raman spectroscopy of isolated silver nanoaggregates*, ChemPhysChem **4**, 1001–1005 (2003).

[33] S. K. Friedlander, *Smoke, dust and haze: Fundamentals of aerosol behavior.* (Wiley, New York, 1977).

[34] CRC, *CRC Handbook of Chemistry and Physics* (CRC Press, Boca Raton, 1997), 78th edn.

[35] I. Egry, G. Lohoefer, and G. Jacobs, *Surface tension of liquid metals: results from measurements on ground and in space*, Phys. Rev. Lett. **75**, 4043–4046 (1995).

[36] K. Nakaso, M. Shimada, K. Okuyama, and K. Deppert, *Evaluation of the change in the morphology of gold nanoparticles during sintering*, J. Aerosol Sci. **33**, 1061–1074 (2002).

Martin Karlsson

[37] V. B. Storozhev, *The liquid-phase sintering and coalescence of small solid particles*, Aerosol Sci. Technol. **34**, 179–185 (2001).

[38] A. P. Weber and S. K. Friedlander, *In situ determination of the activation energy for restructuring of nanometer aerosol agglomerates*, J. Aerosol Sci. **28**, 179–192 (1997).

[39] A. Schmidt-Ott, *New approaches to in situ characterization of ultrafine agglomerates*, J. Aerosol Sci. **19**, 553–557 (1988).

[40] *Webster's Encyclopedic Unabridged Dictionary of the English Language* (Portland House, New York, 1996).

[41] M. H. Magnusson, K. Deppert, and J.-O. Malm, *Single-crystalline tungsten nanoparticles produced by thermal decomposition of tungsten hexacarbonyl*, J. Mater. Res. **15**, 1564–1569 (2000).

[42] K. Okuyama, R. Ushio, Y. Kousaka, J. Seinfeld, and R. Flagan, *Evaluation of fine particle formation by CVD in a laminar-flow aerosol reactor*, Int. Chem. Eng. **32**, 750–758 (1992).

[43] A. G. Nasibulin, O. Richard, E. I. Kauppinen, D. P. Brown, J. K. Jokiniemi, and I. S. Altman, *Nanoparticle synthesis by copper (II) acetylacetonate vapor decomposition in the presence of oxygen*, Aerosol Sci. Technol. **36**, 899–911 (2002).

[44] M. Ullmann, S. K. Friedlander, and A. Schmidt-Ott, *Nanoparticle formation by laser ablation*, J. Nanoparticle Res. **4**, 499–509 (2002).

[45] R. P. Camata, H. A. Atwater, K. J. Vahala, and R. C. Flagan, *Size classification of silicon nanocrystals*, Appl. Phys. Lett. **68**, 3162–3164 (1996).

[46] T. Seto, M. Hirasawa, N. Aya, N. Suzuki, T. Yoshida, Y. Kawakami, and E. Ozawa, *Synthesis of size-selected silicon nanoparticles by laser ablation*, J. Aerosol Sci. **31**, S628–S629 (2000).

[47] M. F. Becker, J. R. Brock, H. Cai, D. E. Henneke, J. W. Keto, J. Lee, W. T. Nichols, and H. D. Glicksman, *Metal nanoparticles generated by laser ablation*, Nanostruct. Mater. **10**, 853–863 (1998).

[48] W. R. Cannon, S. C. Danforth, J. H. Flint, J. S. Haggerty, and R. A. Marra, *Sinterable ceramic powders from laser-driven reactions*, J. Am. Ceram. Soc. **65**, 324–335 (1982).

[49] T. Majima, T. Miyahara, K. Haneda, T. Ishii, and M. Takami, *Preparation of iron ultrafine particles by the dielectric breakdown of Fe(CO)$_5$ using a transversely excited atmospheric CO$_2$ laser and their characteristics*, Jpn. J. Appl. Phys. **33**, 4759–4763 (1994).

[50] S. Veintemillas-Verdaguer, O. Bomati, M. P. Morales, P. E. Di Nunzio, and S. Martelli, *Iron ultrafine nanoparticles prepared by aerosol laser pyrolysis*, Mater. Lett. **57**, 1184–1189 (2003).

[51] F. Huisken, H. Hofmeister, B. Kohn, M. Laguna, and V. Paillard, *Laser production and deposition of light-emitting silicon nanoparticles*, Appl. Surf. Sci. **154**, 305–313 (2000).

[52] A. Galvez, N. Herlin-Boime, C. Reynaud, C. Clinard, and J.-N. Rouzaud, *Carbon nanoparticles from laser pyrolysis*, Carbon **40**, 2775–2789 (2002).

[53] K. Elihn, F. Otten, M. Boman, F. E. Kruis, H. Fissan, and J.-O. Carlsson, *Nanoparticle formation by laser-assisted photolysis of ferrocene*, Nanostruct. Mater. **12**, 79–82 (1999).

[54] K. Takeuchi, Y. Kuga, S. Satooka, and K. Okuyama, *Growth of UF_5 nanoparticles formed by laser photolysis in a supersonic nozzle reactor*, J. Aerosol Sci. **29**, 1027–1033 (1998).

[55] K. Elihn, F. Otten, M. Boman, P. Heszler, F. E. Kruis, H. Fissan, and J.-O. Carlsson, *Size distributions and synthesis of nanoparticles by photolytic dissociation of ferrocene*, Appl. Phys. A **72**, 29–34 (2001).

[56] W. A. Saunders, P. C. Sercel, R. B. Lee, H. A. Atwater, K. J. Vahala, R. C. Flagan, and E. J. Escorcia-Aparcio, *Synthesis of luminescent silicon clusters by spark ablation*, Appl. Phys. Lett. **63**, 1549–1551 (1993).

[57] W. Mahoney and R. P. Andres, *Aerosol synthesis of nanoscale clusters using atmospheric arc evaporation*, Mater. Sci. Eng. A **204**, 160–164 (1995).

[58] W. A. Saunders, P. C. Sercel, H. A. Atwater, K. J. Vahala, and R. C. Flagan, *Vapor phase synthesis of crystalline nanometer-scale GaAs clusters*, Appl. Phys. Lett. **60**, 950–952 (1992).

[59] G. D. Ulrich, *Flame synthesis of fine particles*, Chem. Eng. News **62**, 22–29 (1984).

[60] S. Vemury, S. E. Pratsinis, and L. Kibbey, *Electrically controlled flame synthesis of nanophase TiO_2, SiO_2 and SnO_2 powders*, J. Mater. Res. **12**, 1031–1042 (1997).

[61] S. H. Ehrman, S. K. Friedlander, and M. R. Zachariah, *Characteristics of SiO_2/TiO_2 nanocomposite particles formed in a premixed flat flame*, J. Aerosol Sci. **29**, 687–706 (1998).

[62] R. Mueller, L. Mädler, and S. E. Pratsinis, *Nanoparticle synthesis at high production rates by flame spray pyrolysis*, Chem. Eng. Sci. **58**, 1969–1976 (2003).

[63] R. M. Young and E. Pfender, *Generation and behavior of fine particles in thermal plasmas – a review*, Plasma Chem. Plasma Process. **5**, 1–37 (1985).

[64] D. Vollath and K. E. Sickafus, *Synthesis of nanosized ceramic nitride powders by microwave supported plasma reactions*, Nanostruct. Mater. **2**, 451–456 (1993).

[65] C. Chou and J. Phillips, *Plasma production of metallic nanoparticles*, J. Mater. Res. **7**, 2107–2113 (1992).

[66] M. H. Magnusson, K. Deppert, J.-O. Malm, J.-O. Bovin, and L. Samuelson, *Gold nanoparticles: production, reshaping, and thermal charging*, J. Nanoparticle Res. **1**, 243–251 (1999).

[67] K. Deppert, I. Maximov, L. Samuelson, H.-C. Hansson, and A. Weidensohler, *Sintered aerosol masks for dry-etched quantum dots*, Appl. Phys. Lett. **64**, 3293 (1994).

[68] K. Deppert, J.-O. Bovin, J.-O. Malm, and L. Samuelson, *A new method to fabricate size-selected compound semiconductor nanocrystals: aerotaxy*, J. Crystal Growth **169**, 13–19 (1996).

[69] K. Deppert, M. H. Magnusson, L. Samuelson, J.-O. Malm, C. Svensson, and J.-O. Bovin, *Size-selected nanocrystals of III-V semiconductor materials by the aerotaxy method*, J. Aerosol Sci. **29**, 737–748 (1998).

[70] M. N. A. Karlsson, K. Deppert, L. S. Karlsson, J.-O. Malm, and M. Mühlberg, *Indium-selenium nanoparticles: What is the shape?*, J. Aerosol Sci. **34**, S269–S270 (2003).